Production of highly spin-polarized atomic hydrogen and deuterium by spin-exchange optical pumping

S. G. Redsun,* R. J. Knize,† G. D. Cates, and W. Happer
Physics Department, Princeton University, Princeton, New Jersey 08544
(Received 16 April 1990)

We have produced highly spin-polarized atomic hydrogen by spin-exchange optical pumping. A tunable ring dye laser is used to polarize rubidium atoms by optical pumping. The cell containing the rubidium vapor is coated with paraffin in order to reduce spin relaxation due to wall collisions. Hydrogen gas is dissociated in an inductive discharge and flows continuously through the cell, in which the hydrogen atoms are polarized by spin-exchange collisions with the polarized rubidium atoms. Atomic-hydrogen polarization as high as $2\langle J_z\rangle_H=0.72(6)$ has been observed, which is the highest polarization yet produced by this method. However, the rubidium polarization may be limited to this value due to radiation trapping at higher rubidium densities. The spin-relaxation rate of atomic hydrogen on a paraffin-coated cell is also measured and corresponds to about 7600 wall bounces between wall relaxation.

I. INTRODUCTION

Present interest in spin-polarized atomic hydrogen has been generated by two factors. First, the development of polarized beams and targets has allowed the investigation of spin-dependent phenomena in atomic, nuclear, and high-energy physics. Second, since the hydrogen atom is the simplest atom, it is widely used in experimental tests of theoretical models of atomic and subatomic structure. Polarized atoms may be used to determine atomic energy levels with extreme precision by driving transitions with radio frequency (rf) fields. Spin exchange techniques closely related to those described in this work have been used[1] to measure the ratio of atomic g factors to better than one part in 10^6, and the ground-state hyperfine separation of deuterium to better than four parts in 10^9. In an early application of the hydrogen maser,[2] the ground-state hyperfine separation of H was measured to better than two parts in 10^{11}. Polarized hydrogen has been used as a target in low-, medium-, and high-energy physics. Actual and proposed uses have included the study of spin-dependent effects in atomic scattering,[3] the study of the spin structure of hadrons,[4] and the measurement of spin-dependent nuclear form factors.[5] Polarized tritium would be a very natural system in which to determine the neutrino mass by beta-decay measurements. Polarized hydrogen is also important to the study of degenerate quantum gas phenomena, and is expected to display Bose condensation and other interesting quantum-mechanical properties at cryogenic temperatures and sufficiently high density.[6] Spin-polarized hydrogen is used in order to suppress recombination so that higher concentrations may be attained.

Spin-polarized fusion is a potentially significant application of polarized hydrogen. Since at low energies the fusion reaction $d(t,\alpha)n$ goes almost exclusively through the spin-$\frac{3}{2}$ ^{5}He intermediate resonance state, the reaction rate should be enhanced by a factor of 1.5 if the deuteron and triton spins are aligned. Theoretical calculations for typical magnetic confinement[7] and inertial confinement[8] fusion reactors suggest that the polarization would last long enough in the reactor to make this practical. In addition, the polarization of the reactants would yield better control over the direction of the neutrons and alpha particles produced in the reaction, thereby enhancing their confinement and minimizing radiation damage to the reactor walls. It has been suggested that this effect could also be used to provide intense, well-collimated beams of 14-MeV neutrons for use in medical radiology.[9]

A near-infrared laser with 1 W of output power produces on the order of 4×10^{18} photons per second, giving optical pumping[10] the potential of being a few orders of magnitude more intense than conventional atomic-beam sources of polarized atoms, which are limited to about 10^{15} s^{-1}. In principle, hydrogen atoms could be polarized directly by optical pumping, but there are severe technical problems associated with producing and working with the Lyman-α radiation ($\lambda_{1S\rightarrow2P}=121.6$ nm) necessary to pump hydrogen.[11] cw lasers at the Lyman-α wavelength do not exist, and the fine-structure splitting between the $2\,^2P_{1/2}$ and $2\,^2P_{3/2}$ levels (11 GHz) is smaller than the Doppler broadening of the line at room temperature ($\sim$20 Ghz). This obviates the elimination of D_1 or D_2 resonance radiation for efficient optical pumping.

For these reasons, atomic hydrogen has been polarized by spin exchange with optically pumped alkali atoms. Alkali-hydrogen spin exchange was first used by Anderson *et al.*[12] to measure the hyperfine separations of the hydrogen isotopes. It has subsequently been employed to polarize atomic hydrogen in a sealed cell[13] and in a flowing system presently under development,[14] and also to measure the diffusion constant of atomic hydrogen in helium.[15]

We report here on the polarization of atomic hydrogen by spin-exchange optical pumping. In this experiment, hydrogen gas is dissociated in a glow discharge and flows

continuously through a spin-exchange chamber, where the hydrogen atoms are polarized by spin-exchange collisions with optically pumped rubidium atoms:

$$\mathrm{Rb}(\uparrow)+\mathrm{H}(\downarrow)\rightarrow\mathrm{Rb}(\downarrow)+\mathrm{H}(\uparrow)\ . \quad (1)$$

The hydrogen nucleus is subsequently polarized by the hyperfine interaction, thus $\langle F_z\rangle_H=2\langle J_z\rangle_H=2\langle I_z\rangle_H$, where these are the total, electronic, and nuclear polarizations of the hydrogen, respectively. The measured polarizations are the highest yet achieved using this technique. The chamber walls are coated with paraffin to reduce spin relaxation, which is necessary for the achievement of high polarization. We present measurements of hydrogen and rubidium relaxation on the paraffin wall coatings. We also discuss a novel technique for modifying a ring dye laser in order to obtain suitable optical-pumping light.

II. EXPERIMENTAL APPARATUS

A. Gas flow system

The gas handling system used in this experiment is illustrated in Fig. 1. Hydrogen (or deuterium) gas is purified by passage through a palladium leak, and flows continuously through the system. A Granville-Phillips leak valve controls the gas flow and pressure in the hydrogen lines. The gas lines include getter cells (not shown) containing potassium metal, which are used to remove impurities such as pump oil, water vapor, and other residual gases which evolve from the stainless steel tubing over time. The getters are necessary to prevent depletion of the rubidium in the reservoir.

The hydrogen gas is dissociated in an rf inductive discharge created by a 7-turn copper coil 6 cm in diameter ($\sim 3\ \mu$H), which is part of an LC tuned circuit, suspended around the glass discharge region. The dissociation fraction in the discharge is thought to be above 90%. The discharge region is located about 15 cm from the spin-exchange cell, and is shielded by an aluminum box.

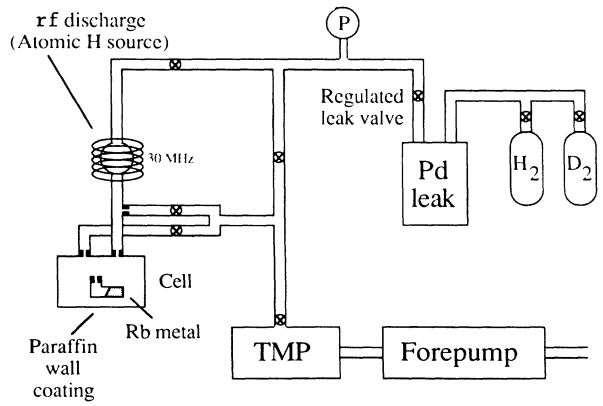

FIG. 1. A schematic representation of the gas flow system. Included in the diagram are the spin-exchange cell (Cell), a turbo-molecular pump (TMP), and a pressure gauge (P).

The hydrogen flow system used in this experiment is similar to that of Hayne *et al.*[1] It consists of a cylindrical Pyrex spin-exchange chamber, 5.1 cm in diameter and 7.6 cm in length, with a sidearm containing natural rubidium metal (isotopic abundance 73% ^{85}Rb and 27% ^{87}Rb). The spin-exchange chamber is separated from the input line, the output line, and the rubidium reservoir by capillary tubes of length ~ 5 mm and respective diameters 0.1, 0.5, and 2.0 mm. It is important that the diameter of the input capillary be less than about 0.2 mm to prevent energetic particles from the hydrogen discharge from entering the cell, where they bombard the cell walls and rapidly damage the paraffin coating. The output lines lead to the turbomolecular (TMP) and mechanical pumps, which remove the gas from the system.

B. Paraffin wall coating

The walls of the chamber are coated with a commercial paraffin mixture (Paraflint) in order to prevent the depolarization of rubidium and hydrogen atoms at the cell walls. Paraffin has the advantages that it can easily be restored from a contaminated state, unlike silicon coatings such as Drifilm and Surfasil, and does not react chemically with alkali metals, as does Teflon. The main disadvantage of Paraflint is that its melting point (~ 105 °C) prevents operation at a temperature higher than that corresponding to a rubidium density of $\sim 10^{12}$ atoms/cm^3. This was not a serious drawback in this work, as the optimum rubidium density was found to be limited to about 10^{11} atoms/cm^3. During the initial preparation, the spin-exchange cell is loaded with several (~ 12) chips of paraffin about 10 mm^2 in size. The paraffin is distributed over the cell walls in two ways: either by baking the cell for several hours at a temperature above the melting point of the paraffin, or by melting local paraffin concentrations with a heat gun for about one minute. In either case, the coated cell will have a slightly frosty appearance due to the paraffin film on the cell walls. This process is repeated as necessary if the coating becomes degraded as evidenced by the increase in the wall relaxation rate.

C. Temperature control system

Temperature regulation of the system is achieved by enclosing the spin-exchange cell in an oven, heated by hot air flow. The oven has glass windows for transmission of the pumping and fluorescent light. A temperature gradient is maintained between the rubidium reservoir and the spin-exchange cell by enclosing the reservoir in a jacket through which cooling air flows. This two-temperature system significantly reduces the deposition of rubidium on the walls of the main cell by causing the Rb to collect in the colder reservoir, thus preventing contamination of the wall coating.

The cell and reservoir temperatures are measured by thermocouples mounted near the spin-exchange cell and inside the reservoir jacket, respectively. The rubidium density in the reservoir is obtained from the experimental temperature dependence of the vapor density as determined by Killian,[16] whose empirical formula is

$$\log_{10}[\mathrm{Rb}] = 26.41 - \frac{4132}{T} - \log_{10} T \ , \tag{2}$$

where [Rb] is in atoms/cm^3 and T is in K. The rubidium density in the spin-exchange cell is slightly lower, and is given approximately by

$$[\mathrm{Rb}]_c = [\mathrm{Rb}]_r \frac{C_r}{C_r + C_i + C_0 + V/\tau_a} \ , \tag{3}$$

where C_r, C_i, and C_0 are the conductances of the reservoir, input, and output capillaries, respectively, $V \approx 150$ cm^3 is the cell volume, and $\tau_a \sim 100$ sec (Ref. 17) is the mean time before an alkali atom is absorbed by the paraffin-coated wall. The gas kinetics in the capillaries are dominated by free molecular flow, and the capillary conductances at 350 K are given approximately by[18]

$$C = \frac{5 \times 10^4 \ \mathrm{cm^3 \, sec^{-1}}}{\sqrt{m}} \frac{D^3}{L} \ , \tag{4}$$

where D and L are the diameter and length of the capillary tube, and m is the atomic mass of the atom or molecule. Substitution of the appropriate numbers in (3) and (4) yields $[\mathrm{Rb}]_c = 0.98[\mathrm{Rb}]_r$.

D. Optical-pumping–polarization technique

The polarization and detection aparatus used in this experiment are shown in Fig. 2. We used a Coherent 699-21 ring dye laser with LD-700 dye, pumped by a Spectra-Physics 171 krypton ion laser (~5W), tuned to the rubidium D_1 line at 794.8 nm. The ring dye laser was operated in two distinct configurations. In the single frequency configuration, etalons were inserted into the cavity, and the laser was actively locked to a single frequency with a resulting linewidth of about 1 MHz. In the broadband configuration, the etalons were not used, and a novel technique was employed that resulted in a fairly homogeneous frequency spectrum with about a 10-GHz bandwidth. The laser is equipped with a Brewster plate which, when operating in a single frequency configuration, is used for scanning the frequency by amounts up to 30 GHz. When the Brewster plate is tilted, it changes the length of the laser cavity, hence shifting the frequency of each individual cavity mode. We applied an audio frequency (about 1 kHz) voltage to the Brewster plate, taking care to tune the frequency to match the natural resonant frequency for the device. Modulating the Brewster plate in this way causes very large frequency shifts of the individual cavity modes, forcing the laser to hop back and forth between cavity modes with time scales that are fast compared to the drive frequency. We used a Fabry-Pérot interferometer to study the frequency spectrum of the laser. When the Brewster plate was not used, the laser would lase in several cavity modes simultaneously, and frequent hopping would occur. Optical pumping was impractical in this case. When the audio frequency was applied to the Brewster plate the mode structure observed with the Fabry-Pérot would break up into what appeared to be random noise over many GHz, and we were able to optically pump both hyperfine multiplets of the Rb.

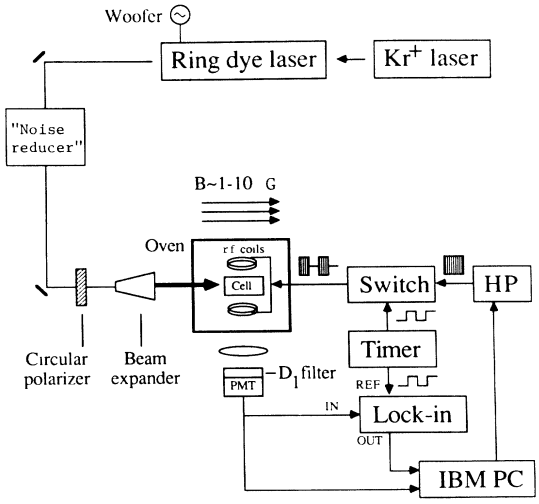

FIG. 2. A schematic representation of the polarization and detection apparatus. In the configuration shown, optical pumping was accomplished using a ring dye laser. Included in the diagram are a Hewlett Packard Model No. 3325A frequency synthesizer (HP) that was used for generating an oscillating magnetic field, and an IBM model XT personal computer (IBM XT) that was used for data collection. The fluorescence from the Rb vapor was detected by a photomultiplier tube (PMT) equipped with an interference filter that selectively transmitted the Rb D_1 line (D_1 filter).

The intensity of the pumping light is kept constant to within a few percent by a Coherent 307 noise reducer, which splits off part of the beam to provide feedback to an electro-optic modulator through which the main beam travels. The beam then passes through a quartz quarter-wave plate ($\lambda/4$ at 800 nm) and is expanded to about 2.5 cm diameter before entering the main cell. A trio of orthogonal Helmholtz coils cancel out the earth's magnetic field and maintain a constant longitudinal magnetic field B of a few gauss, which corresponds to the polarization axis of the circularly polarized photons.

III. EXPERIMENTAL RESULTS

A. Rubidium wall relaxation

The average rubidium wall relaxation rate γ_{Rb} is measured by monitoring the transmission of circularly polarized light though the cell as the vapor becomes polarized. A rubidium vapor lamp[19] may be used for this purpose. Such lamps have the advantages of very low intensity fluctuations (shot-noise limited) and reasonably complete Doppler and hyperfine frequency coverage due to pressure broadening by the inert gas and the discharge in the bulb. Some of the light travels through an interference filter that selectively passes the rubidium D_1 line but blocks the D_2 line, and then continues through a circular polarizer before being focused into the cell by a spherical lens. The transmitted light is focused by another spherical lens onto a photomultiplier tube detector.

The transmission I_T through a cell of length L and polarization $\langle J_z \rangle$ is

$$I_T = I_0 e^{-[\mathrm{Rb}]\sigma L(1-2\langle J_z\rangle)} \tag{5}$$

where σ is the absorption cross section and I_0 is the intensity of the pumping light. If the cell is optically thin ($[\mathrm{Rb}]\sigma L < 1$), then we can express the time dependence of the transmitted light by

$$\frac{d}{dt} I_T \approx 2[\mathrm{Rb}]\sigma L I_T \frac{d}{dt}\langle J_z\rangle \ . \tag{6}$$

We therefore assume that the transmitted light closely tracks the rubidium polarization. The time evolution of the rubidium and hydrogen polarizations may be qualitatively described by a simple model which ignores the nuclear spin:

$$\frac{d\langle J_z\rangle_{\mathrm{Rb}}}{dt} = \frac{\Gamma}{3}(1-2\langle J_z\rangle_{\mathrm{Rb}}) - \gamma'_{\mathrm{Rb}}\langle J_z\rangle_{\mathrm{Rb}} - [\mathrm{H}]\langle\sigma v\rangle(\langle J_z\rangle_{\mathrm{Rb}} - \langle J_z\rangle_{\mathrm{H}}) \ , \tag{7}$$

$$\frac{d\langle J_z\rangle_{\mathrm{H}}}{dt} = -\gamma'_{\mathrm{H}}\langle J_z\rangle_{\mathrm{H}} - [\mathrm{Rb}]\langle\sigma v\rangle(\langle J_z\rangle_{\mathrm{H}} - \langle J_z\rangle_{\mathrm{Rb}}) \ , \tag{8}$$

where Γ is the average absorption rate for unpolarized atoms, γ'_{Rb} and γ'_{H} are the measured spin-relaxation rates for rubidium and hydrogen, [H] and [Rb] are the hydrogen and rubidium concentrations, and $\langle\sigma v\rangle$ is the velocity-averaged Rb-H binary spin-exchange cross section. The measured relaxation rates $\gamma'_{\mathrm{Rb,H}}$ are the sum of the wall relaxation rates $\gamma_{\mathrm{Rb,H}}$ and the rates at which the atoms escape the cell, $\gamma_{e(\mathrm{Rb,H})}$:

$$\gamma_e = \frac{2\bar{v}A_c}{3\pi V} \ , \tag{9}$$

where A_c is the total area of all the capillary apertures, V is the cell volume, and $\bar{v}$ is the average atomic velocity. We find $\gamma_e = 1.3\ \mathrm{sec}^{-1}$ for rubidium and $12\ \mathrm{sec}^{-1}$ for hydrogen atoms.

In the absence of atomic hydrogen, the rubidium polarization evolves as

$$2\langle J_z\rangle_{\mathrm{Rb}}(t) = \frac{2\Gamma/3}{2\Gamma/3+\gamma'_{\mathrm{Rb}}}(1-e^{-(2\Gamma/3+\gamma'_{\mathrm{Rb}})t}) \ . \tag{10}$$

It can be shown that due to the nonzero nuclear spin, the slowest exponential rate actually has the value $f_I(2\Gamma/3+\gamma_{\mathrm{Rb}})$ (neglecting capillary losses), where $f_I = 2(2I+1)^{-2}$ is the correction factor due to the nuclear spin in the limit of slow spin exchange.[20,21] Hence the buildup of the transmitted light may be described by a single exponential after sufficient time has elapsed for the faster exponentials to decay.

To observe the time dependence of the transmitted light, the rubidium atoms are first depolarized by application of an rf pulse of duration ~ 100 msec at the frequency of the ^{85}Rb hyperfine Zeeman transitions. In a longitudinal magnetic field of about 0.65 G, this means $\omega \approx 300$ kHz. This magnetic field strength is too low for the individual Zeeman transitions to be resolved, so all of the $\Delta m_F = \pm 1$ transitions will be driven and the ^{85}Rb will become completely depolarized. When the depolarizing rf is switched off, the rubidium polarization is allowed to buildup until well after it reaches equilibrium, typically for 500 or 1000 msec. The sequence of a short Zeeman pulse followed by a long polarization buildup is repeated many times in order to signal average the transmitted light, as shown in Fig. 3. The curve of transmission versus time is then fit to a single exponential, beginning the fit at a point where enough time has elapsed that the faster exponentials have decayed away. The spin-relaxation rate γ'_{Rb} is extracted from the total exponential rate by taking a series of rate measurements such as the one shown in Fig. 3, using neutral density filters to attenuate the lamp beam by different factors for each measurement, and extrapolating these measured exponential rates to zero pumping light. Such a linear extrapolation is shown in Fig. 4. In general, the rate measurements were made at room temprature in order to ensure that the rubidium vapor was optically thin.

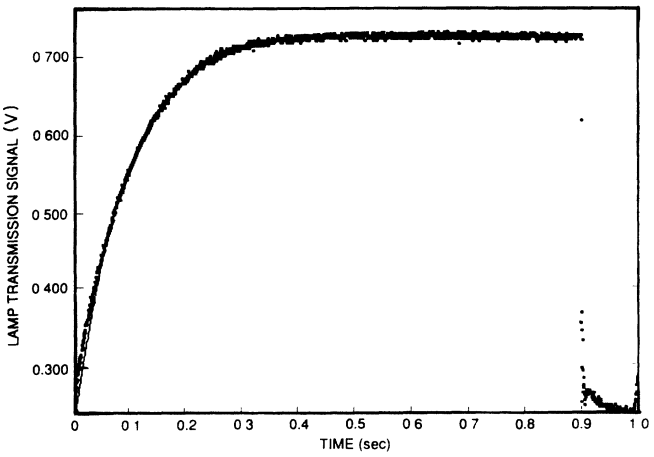

FIG. 3. Exponential rise curve of the transmitted light vs time, corresponding to the exponential rise of the rubidium polarization following a depolarizing rf pulse. The rate constant is $2\Gamma/3+\gamma'_{\mathrm{Rb}} = 11.0\ \mathrm{sec}^{-1}$ in this case.

The slowest relaxation rate observed in a recently cured cell at room temperature was $2.1\ \mathrm{sec}^{-1}$, while rates

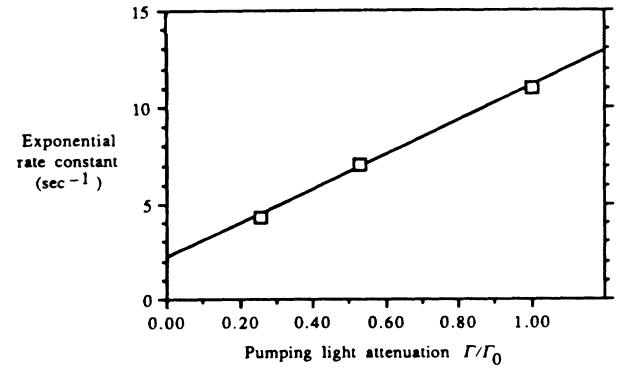

FIG. 4. Exponential rise constant of the transmission, plotted vs the attenuation of the pumping light. The y intercept is the measured relaxation rate $\gamma'_{\mathrm{RB}} = 2.1\ \mathrm{sec}^{-1}$.

of 2.5 sec^{-1} or better were typical after curing. Correcting for the capillary loss rate, this works out to $\gamma_{Rb}=0.8-1.2$ sec^{-1} for typical good wall coatings. For a cylindrical cell, the mean number of bounces between wall relaxation is

$$N_{Rb}=\frac{\bar{v}_{Rb}(R+L)}{2\gamma_{Rb}RL} , \tag{11}$$

where R and L are the cell radius and length. Hence these rates correspond to about 6300–9000 wall bounces before randomization of the rubidium atomic spin F_z. This is an order of magnitude of more bounces than the numbers reported for sodium[22] and potassium[14] on silicone wall coatings.

B. Hydrogen concentration and flow rate

The atomic hydrogen concentration in the spin-exchange cell may also be estimated by this method, as the spin-exchange rate $[H]\langle\sigma v\rangle/18$ adds to the exponential time constant when the dissociator is on (where $f_I=\frac{1}{18}$ is the nuclear-spin correction factor for ^{85}Rb). We estimate $[H]_c$ using the value of the Rb-H spin-exchange rate constant $\langle\sigma v\rangle=5.5\times10^{-10}$ $cm^3\,sec^{-1}$.[23] Under typical conditions the increase in the exponential rate is on the order of 5 sec^{-1}, so we get $[H]_c$ on the order of 10^{11} atoms/cm^3.

The flow rate of atomic hydrogen through the spin-exchange cell Φ_H is estimated from the atomic hydrogen concentration $[H]_c$ and the output capillary conductance C_0:

$$\Phi_H\approx[H]_cC_0 . \tag{12}$$

Using the cell geometry, this yields $\Phi_H\sim10^{12}$ H atoms/sec for $[H]_c\sim10^{11}$ atoms/cm^3. The molecular hydrogen concentration in the spin-exchange cell is given approximately by

$$[H_2]_c\approx\frac{P_d}{k_BT}\frac{C_i}{C_0}-\frac{[H]_c}{2} , \tag{13}$$

where P_d is the pressure in the hydrogen discharge and C_i is the input capillary conductance. For $P_d\sim0.2$ torr we get $[H_2]_c\sim10^{14}$ atoms/cm^3, equivalent to a few millitorr. The ratio of atomic to molecular hydrogen in the main cell is thus on the order of 10^{-3}. In the future, it would be desirable to have direct measurements of these densities.

C. Atomic hydrogen polarization: signal detection

The atomic polarizations are measured by a magnetic resonance technique which employs optical detection of the Rb fluorescence. Upon absorption of the D_1 pumping light, the rubidium atoms in the cell are excited to the $^2P_{1/2}$ state and then undergo spontaneous radiative decay to the ground state. Since the absorption of circularly polarized light is proportional to $(1-2\langle J_z\rangle_{Rb})$, and a photon is emitted for each absorbed photon, the fluorescence is also proportional to $(1-2\langle J_z\rangle_{Rb})$, where $\langle J_z\rangle_{Rb}$ is the rubidium electron polarization.

The hydrogen or deuterium polarization is deduced from the changes in the fluorescence that occur when depolarizing rf is applied at a frequency corresponding to the $\Delta F=0$ and $\Delta m_F=\pm1$ transitions between the hydrogen or deuterium hyperfine Zeeman sublevels. Depolarizing the hydrogen or deuterium affects the Rb polarization by creating an additional sink for the Rb angular momentum. The depolarizing rf is chopped at 2.5–5.0 Hz, and the chopping frequency is used as the reference signal for a lock-in amplifier. The rf frequency is swept through the Zeeman transitions at a sufficiently high magnetic field so that the individual transitions are resolved. An example of the lock-in output during a hydrogen polarization measurement is shown in Fig. 5, which was obtained us-

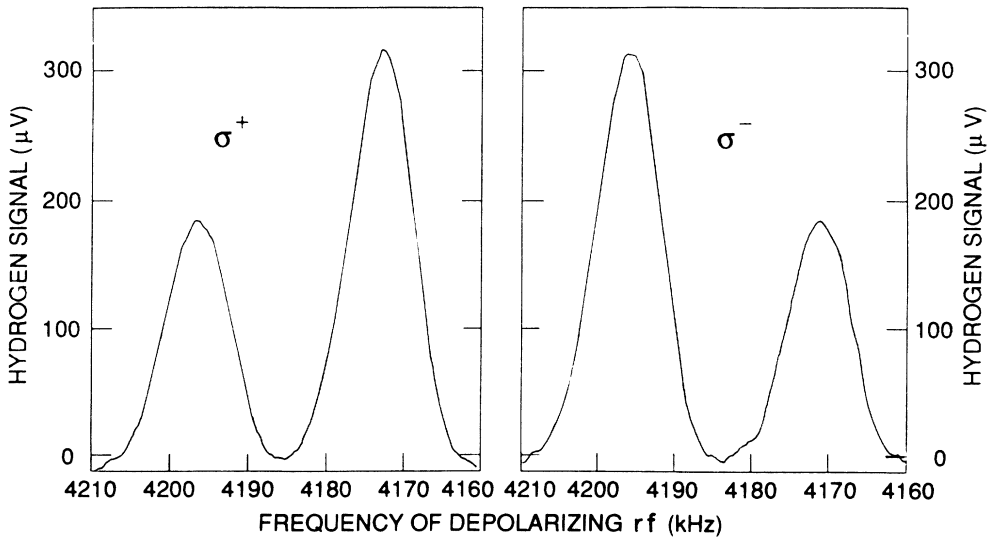

FIG. 5. Hydrogen signals obtained by pumping with the Rb resonance lamp. The polarization is $2\langle J_z\rangle_H=0.24$. These scans were taken with a cell temperature of 74 °C, a Rb reservoir temperature of 47 °C, an rf discharge power of 60 W, and an rf discharge pressure of 0.16 Torr.

ing a Rb resonance lamp as the optical pumping light source. The Zeeman transitions are driven by a transverse oscillating magnetic field created by a pair of rf coils, as indicated in Fig. 2. Since the spin exchange rates are typically above 50 Hz and the rf is off for several time constants, there is adequate time for the polarization to build up.

The Rb fluorescence signal S is proportional to the net number of hydrogen or deuterium spins flipped by the Zeeman rf, thus[24]

$$S \propto |\langle F, m_F - 1 | J_x | F, m_F \rangle|^2 (n_{F,m_F} - n_{F,m_F-1}) , \quad (14)$$

where J_x is the x component of the angular momentum operator **J**, and n_{F,m_F} is the sublevel population. This expression is only valid in the limit of low rf power. The square of the matrix element of J_x is proportional to $(F+m_F)(F+1-m_F)$, which in the case of hydrogen is equal to 2 for both transitions of interest. Thus, for hydrogen, $S \propto (n_{F,m_F} - n_{F,m_F-1})$.

Under our experimental conditions, the hydrogen or deuterium sublevel populations are expected to be in a spin-temperature equilibrium,[12] and can thus be described by a single spin temperature parameter β according to the relation

$$n_{F,m_F} = \frac{e^{\beta m_F}}{\sum_{F,m_F} e^{\beta m_F}} . \quad (15)$$

Narrowing our attention to hydrogen, we define S_1 and S_2 to be the Rb fluorescence signals corresponding to the Zeeman transitions $m_F = 1 \leftrightarrow m_F = 0$ and $m_F = 0 \leftrightarrow m_F = -1$, respectively, and we use (14) and (15) to obtain the ratio

$$\frac{S_1}{S_2} = \frac{e^{\beta} - 1}{1 - e^{-\beta}} = e^{\beta} . \quad (16)$$

The measured value of $\beta = \ln(S_1/S_2)$ is used to determine the hydrogen polarization:

$$2\langle J_z \rangle_H = n_{(1,1)} - n_{(1,-1)} = \tanh\frac{\beta}{2} . \quad (17)$$

The uncertainty in the hydrogen polarization is given by

$$\Delta(2\langle J_z \rangle_H) = \frac{1}{2} \frac{\Delta S}{\sqrt{S_1^2 + S_2^2}} \operatorname{sech}^2\frac{\beta}{2} , \quad (18)$$

where ΔS is the noise level.

D. Hydrogen and deuterium signals with lamp pumping

The rubidium resonance lamp is an extremely stable light source, and thus provided a valuable means for studying the polarized-hydrogen signals in addition to the laser. When the signal-to-noise ratio of the lamp signals was too low, the laser signals would inevitably be prohibitively noisy. Figure 5 shows typical lamp-pumping hydrogen signals for both helicities of the pumping light. When the circular polarizer is rotated through 90°, the helicity of the pumping light is reversed and the relative signal heights are inverted. In this case, the hydrogen polarization is $2\langle J_z \rangle_H = 0.24$. For good paraffin coatings, we typically get hydrogen polarizations of $2\langle J_z \rangle_H = 0.20 - 0.25$ with the lamp (total incident power ~ 10 μW). These polarization are comparable to those achieved by Holt *et al.* using laser optical pumping in similar experiments in which silicone wall coatings are used.[25] We note, though, that in the work by Holt *et al.* the hydrogen densities were considerably higher than was the case for the measurements shown in Fig. 5. Nevertheless, these lamp results demonstrate the advantages of the paraffin wall coating.

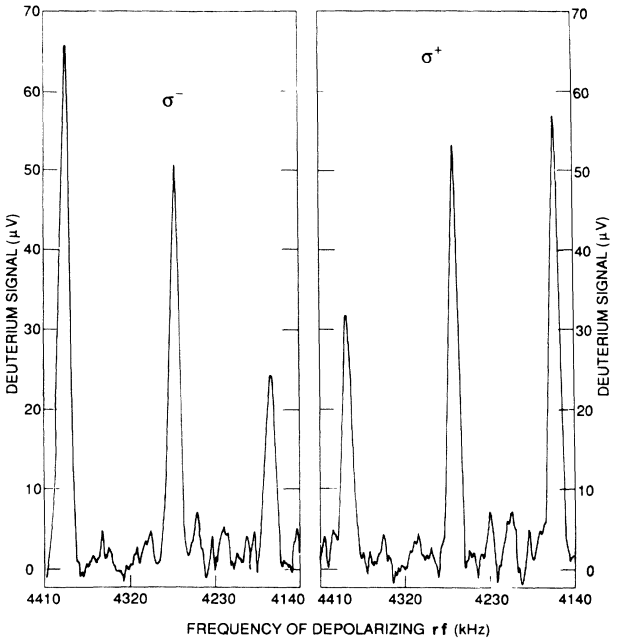

FIG. 6. Deuterium signals by lamp pumping. The polarization is about $2\langle J_z \rangle_D = 0.20$. These scans were taken with a cell temperature of 74 °C, a Rb reservoir temperature of 48 °C, an rf discharge power of 68 W, and an rf discharge pressure of 0.21 Torr.

We have also polarized atomic deuterium with the resonance lamp, and get polarizations of about $2\langle J_z \rangle_D = 0.20$, as shown in Fig. 6. Although there are four possible hyperfine Zeeman transitions in deuterium, there are only three signals because the two $m_F = \frac{1}{2} \leftrightarrow -\frac{1}{2}$ transitions are not resolved. This suggests that the wall relaxation and spin-exchange properties of deuterium are not significantly different from those of hydrogen, and that this spin-exchange polarization technique is of comparable efficiency for all the hydrogen isotopes.

E. Hydrogen signals with laser pumping

Given the result $2\langle J_z \rangle_H = 0.25$ for < 10-μW lamp pumping, one would expect to obtain a very high polarization using a single-frequency ring dye laser with ~ 100 mW of power. The hydrogen signals obtained by pumping with the ring dye laser locked to a single frequency are shown in Fig. 7. The noise level is about as low as the noise in the lamp signals. The polarization is only $2\langle J_z \rangle_H = 0.45(1)$ for the single-mode laser. The unex-

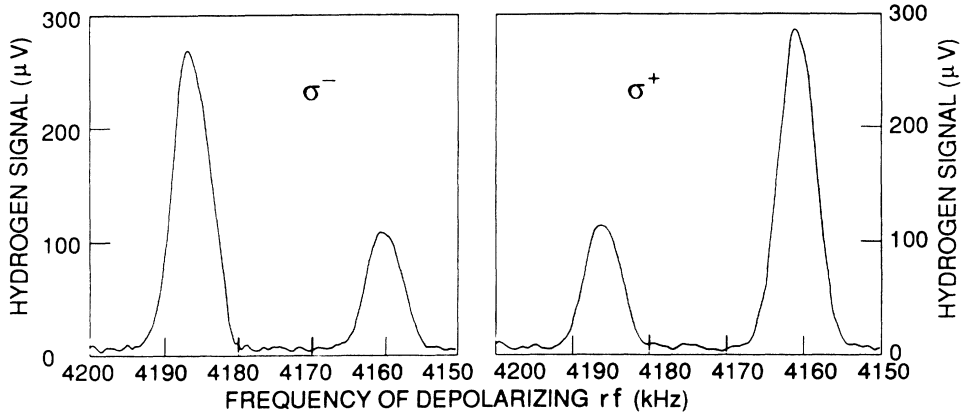

FIG. 7. Hydrogen signals obtained by optical pumping with the ring dye laser in single-frequency configuration. The polarization is $2\langle J_z\rangle_H=0.45$. These scans were taken with a cell temperature of 79 °C, a Rb reservoir temperature of 52 °C, an rf discharge power of 2.0 W, and an rf discharge pressure of 0.215 Torr.

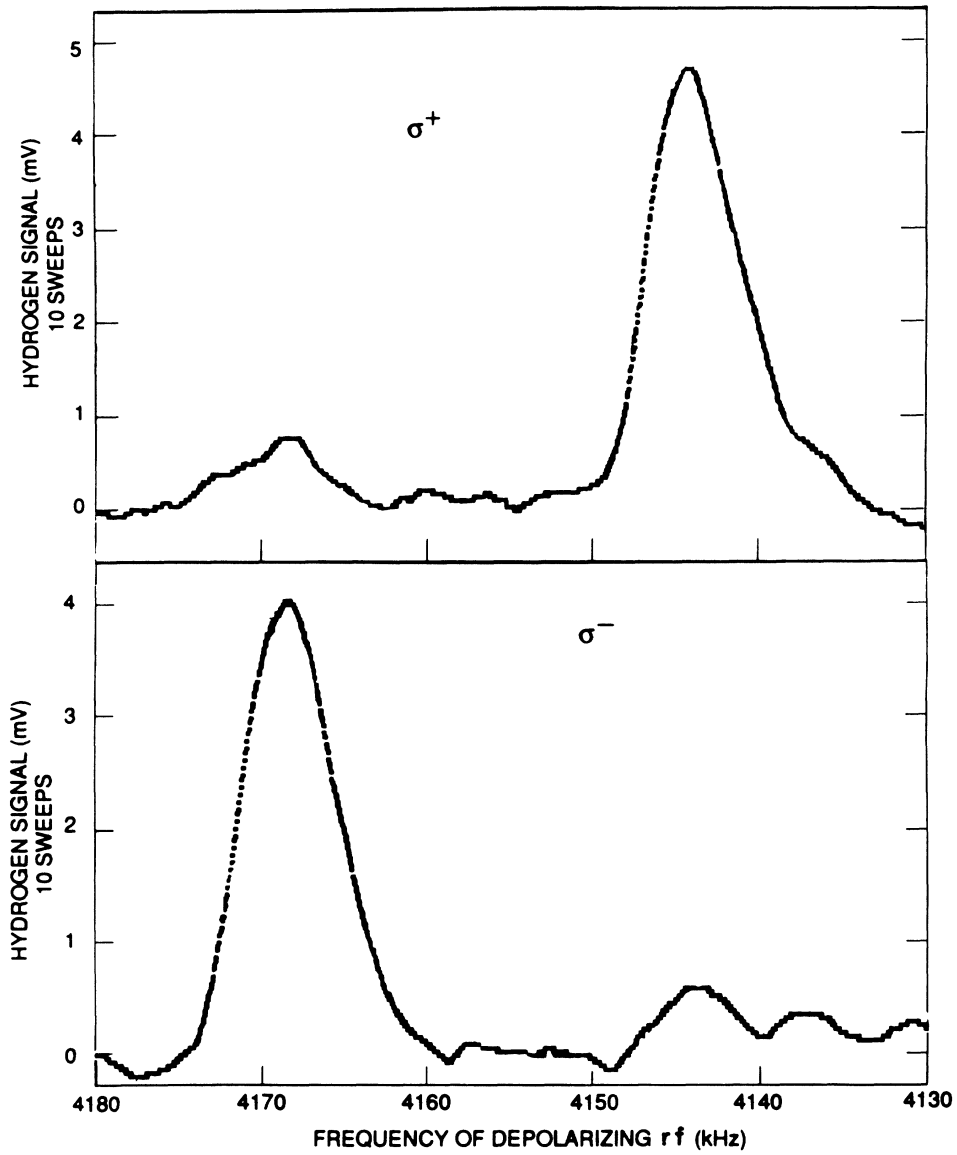

FIG. 8. Computer digitized and averaged hydrogen signals obtained by optical pumping with the ring dye laser in the broadband frequency-jittered configuration. These traces are each the average of 10 sweeps. The average polarization for the two sweeps is $2\langle J_z\rangle_H=0.67(10)$. These scans were taken with a cell temperature of 83 °C, a Rb reservoir temperature of 52 °C, an rf discharge power of 2.5 W, and an rf discharge pressure of 0.30 Torr.

pectedly low polarization is due to selective hyperfine pumping. Since the laser is only about 1 MHz in width in this configuration, and the hyperfine separation in Rb is several GHz, we are only able to pump out of one hyperfine multiplet. With the frequency tuned to pump the lower hyperfine multiplet, we typically get $2\langle J_z\rangle_H = 0.40-0.45$, but we get $2\langle J_z\rangle_H < 0.10$ when pumping the upper hyperfine multiplet. This is in reasonable agreement with calculations.

In order to obtain adequate hyperfine coverage, we used the laser frequency-jittering technique mentioned earlier, in which the scanning Brewster plate is driven to smoothly vary the cavity length, resulting in a fairly smooth distribution of the frequency spectrum of the output beam. A typical pair of laser hydrogen signals obtained using this technique is shown in Fig. 8. From the relative heights of the peaks, the average atomic hydrogen polarization is determined to be $2\langle J_z\rangle_H = 0.67(10)$. Both of the traces shown in Fig. 8 are the average of ten sweeps. The hydrogen polarization produced with the laser in the frequency-jittered configuration was typically $2\langle J_z\rangle_H \sim 0.60-0.70$. The best polarization was 0.72(6).

In addition to the laser power fluctuations and frequency drift, another important source of systematic uncertainty in this experiment is that the Zeeman rf partially depolarizes the atoms, so the polarization we measure is always somewhat less than the true equilibrium polarization. This is equivalent to the statement that Eq. (14) is valid in the limit of low rf power. To illustrate this effect, a typical measurement of the Zeeman rf amplitude dependence of the hydrogen polarization (produced by lamp pumping, in this case) is shown in Fig. 9. The laser-polarized hydrogen signals shown in Figs. 7 and 8 were acquired with the depolarizing rf amplitude set as low as possible. Therefore, the polarization values we report are thought not to be significantly underestimated. Also, since the lock-in averages during a period when the polarization starts at zero and builds up to its steady-state value, the measured polarizations may be underestimated by several percent.

F. Hydrogen wall relaxation

We may use the highest laser polarization measurements to estimate γ_H. The steady-state hydrogen polarization is given by

$$\frac{\langle J_z\rangle_H}{\langle J_z\rangle_{Rb}} = \frac{[Rb]\langle\sigma v\rangle}{[Rb]\langle\sigma v\rangle + \gamma'_H} . \tag{19}$$

We have measured the rubidium polarization to be about $2\langle J_z\rangle_{Rb} = 0.90$, and the hydrogen polarization to be about $2\langle J_z\rangle_H = 0.70$. With a spin-exchange rate $[Rb]\langle\sigma v\rangle = 110\ \text{sec}^{-1}$, we use (19) to find that $\gamma'_H = 31\ \text{sec}^{-1}$. By Eq. (9), the capillary loss rate for hydrogen is about $12\ \text{sec}^{-1}$. Subtracting this from the measured rate, we get for the wall relaxation rate $\gamma_H = 19\ \text{sec}^{-1}$. Insertion of the hydrogen numbers in Eq. (11) yields $N_H = 7600$ wall bounces on paraffin. This is comparable to the $\sim 10^4$ wall bounces reported by Goldenberg *et al.*[26] for hydrogen in a paraffin-coated cell.

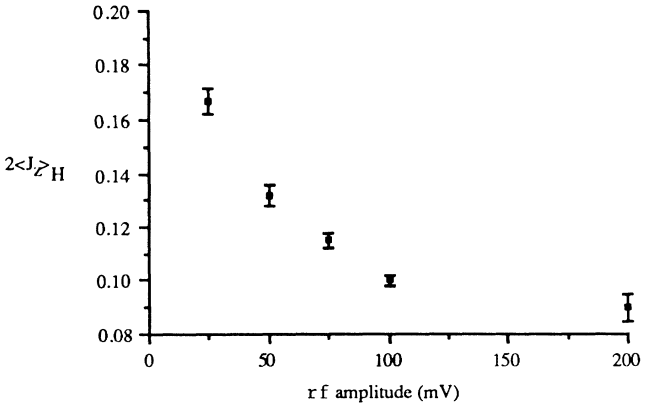

FIG. 9. Dependence of the hydrogen polarization on the amplitude of the depolarizing rf. The rf must be minimized because the magnetic resonance fields used to measure $\langle J_z\rangle$ tend to reduce $\langle J_z\rangle$.

G. Radiation trapping limit

Given our high laser pumping rates and low wall relaxation rates, one would expect to be able to increase the hydrogen polarization by increasing the rubidium density, thereby increasing the spin-exchange rate. However, we observe a severe diminuation of the hydrogen signals at rubidium densities above $\sim 2\times 10^{11}$ atoms/cm^3. We attribute this to radiation trapping, in which the optically thick rubidium vapor is depolarized by multiply scattered photons. Figure 10 illustrates the theoretical limit of spin-exchange optical pumping due to radiation trapping. The curve of $\langle J_z\rangle_{Rb}$ versus temperature is calculated by a Monte Carlo simulation of radiation trapping.[27] The curve of $\langle J_z\rangle_H/\langle J_z\rangle_{Rb}$ versus temperature is obtained from Eq. (19) assuming that the Rb density is given by Eq. (2), $\langle\sigma v\rangle = 5.5\times 10^{-10}\ \text{cm}^3\,\text{sec}^{-1}$ and $\gamma_H = 20\ \text{sec}^{-1}$.

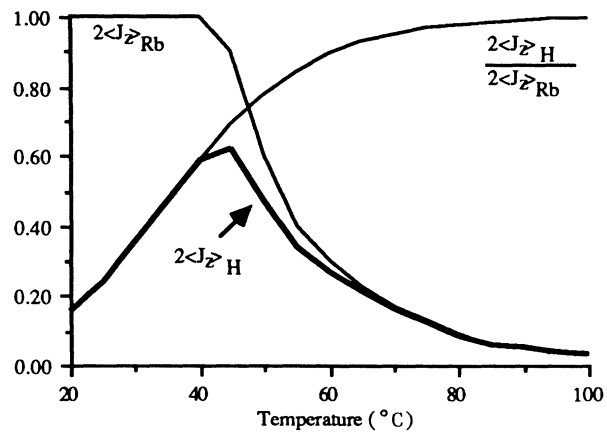

FIG. 10. Calculated Rb and hydrogen polarizations as a function of temperature. Although spin exchange becomes more efficient as the temperature increases, the alkali-metal polarization decreases due to radiation trapping. the maximum hydrogen polarization is obtained between the two extremes.

The bold-style curve of $\langle J_z \rangle_H$ versus temperature is the product of these two. The calculations indicate that the optimum rubidium density for spin-exchange optical pumping of hydrogen with our experimental setup is about 10^{11} atoms/cm^3, which corresponds to $T=45$ °C. The theoretical hydrogen polarization peaks at about $2\langle J_z \rangle_H=0.62$, which is comparable to the highest polarization produced experimentally, $2\langle J_z \rangle_H=0.72$. The difference may be due to underestimation of $\langle \sigma v \rangle$, which is only known to about a factor of 2. For $\langle \sigma v \rangle = 10^{-9}$ cm^3 sec^{-1}, the peak hydrogen polarization would be $2\langle J_z \rangle_H=0.72$, which is in better agreement with our observations. Further experiments could be desirable to examine this problem of radiation trapping.

IV. CONCLUSIONS

We have shown that it is possible to produce highly spin-polarized atomic hydrogen by spin-exchange optical pumping with Rb. The technique for preparing and maintaining high-quality paraffin wall coatings has led to low wall relaxation rates, which allow the rubidium atoms about 9000 bounces and the hydrogen atoms about 7600 bounces before randomization of F_z. We have achieved atomic hydrogen polarization as high as $2\langle J_z \rangle_H=0.72(6)$. In principle, this method of polarization may be used to produce highly polarized deuterium and tritium atoms. We believe that the hydrogen polarization is presently limited by radiation trapping at high rubidium densities.

---

*Present address: Laboratoire de Spectroscopie Hertzienne de l'Ecole Normale Supérieure, Paris 05, France.

†Present address: Physics Department, University of Southern California, Los Angeles, CA 90089.

[1]G. S. Hayne, E. S. Ensberg, and H. G. Robinson, Phys. Rev. **171**, 20 (1968); C. E. Johnson and H. G. Robinson, Phys. Rev. Lett. **45**, 250 (1980).

[2]S. B. Crampton, D. Kleppner, and N. F. Ramsey, Phys. Rev. Lett. **11**, 338 (1963).

[3]G. D. Fletcher, M. J. Alguard, T. J. Gay, V. W. Hughes, P. F. Wainwright, M. S. Lubell, and W. Raith, Phys. Rev. A **31**, 2854 (1985).

[4]M. W. Alguard *et al.*, Phys. Rev. Lett. **37**, 1258 (1976); **37**, 1261 (1976).

[5]R. J. Holt, M. C. Green, L. Young, R. S. Kowalczyk, D. F. Geesaman, B. Zeidman, L. S. Goodman, and J. Napolitano, Nucl. Phys. A **446**, 389C (1985).

[6]I. F. Silvera and J. T. M. Walraven, Prog. Low Temp. Phys. **10**, 139 (1986).

[7]R. M. Kulsrud, H. P. Furth, E. J. Valeo, and M. Goldhaber, Phys. Rev. Lett. **49**, 1248 (1982).

[8]R. M. More, Phys. Rev. Lett. **51**, 396 (1983).

[9]H. Hasuyama and Y. Wakuta, Helv. Phys. Acta **59**, 723 (1986).

[10]W. Happer, Rev. Mod. Phys. **44**, 169 (1972).

[11]T. McIlrath, Ph.D. thesis, Princeton University, 1966.

[12]L. W. Anderson, F. M. Pipkin, and J. C. Baird, Phys. Rev. **120**, 1279 (1960).

[13]R. J. Knize and J. L. Cecchi, Phys. Lett. **113A**, 255 (1985).

[14]L. Young, R. J. Holt, M. C. Green, and R. S. Kowalczyk, Nucl. Instrum. Methods B **24/25**, 963 (1987).

[15]S. G. Redsun and R. J. Knize, Phys. Rev. A **37**, 737 (1988).

[16]T. J. Killian, Phys. Rev. **27**, 578 (1926).

[17]V. Liberman and R. J. Knize, Phys. Rev. A **34**, 5115 (1986).

[18]C. Kittel and H. Kroemer, *Thermal Physics* (Freeman, San Francisco, 1980), Chap. 14.

[19]W. E. Bell, A. L. Bloom, and J. Lynch, Rev. Sci. Instrum. **32**, 688 (1961).

[20]M. A. Bouchiat and J. Brossel, Phys. Rev. **147**, 41 (1966).

[21]X. Zeng, Z. Wu, T. Call, E. Miron, D. Schreiber, and W. Happer, Phys. Rev. A **31**, 260 (1985).

[22]D. R. Swenson and L. W. Anderson, Nucl. Instrum. Methods B **29**, 627 (1988).

[23]H. R. Cole and R. E. Olson, Phys. Rev. A **31**, 2137 (1985).

[24]L. W. Anderson and A. T. Ramsey, Phys. Rev. **132**, 712 (1963).

[25]R. Holt and L. Young (private communication).

[26]H. M. Goldenberg, D. Kleppner, and N. F. Ramsey, Phys. Rev. Lett. **5**, 361 (1960).

[27]S. G. Redsun, Ph.D. thesis, Princeton University, 1990.

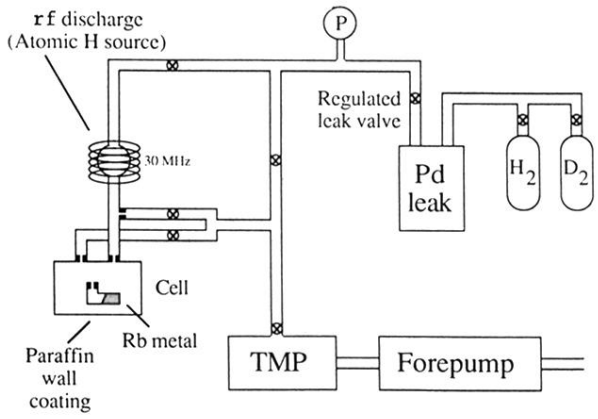

FIG. 1. A schematic representation of the gas flow system. Included in the diagram are the spin-exchange cell (Cell), a turbo-molecular pump (TMP), and a pressure gauge (P).